PAPER • OPEN ACCESS

Impact of spot reduction on the effectiveness of rescanning in pencil beam scanned proton therapy for mobile tumours

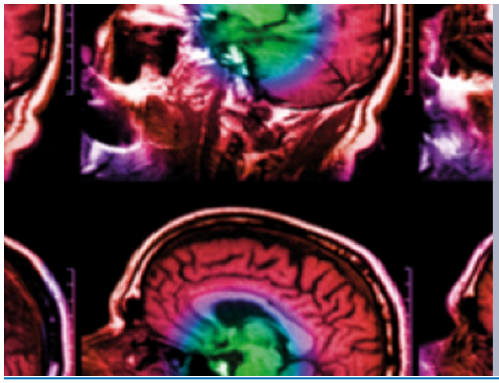

IOP Publishing Phys. Med. Biol. 67 (2022) 215019 https://doi.org/10.1088/1361-6560/ac96c5

Physics in Medicine & Biology

IPEM Institute of Physics and Engineering in Medicine

OPEN ACCESS

RECEIVED
25 April 2022

REVISED
18 September 2022

ACCEPTED FOR PUBLICATION
30 September 2022

PUBLISHED
2 November 2022

PAPER

Impact of spot reduction on the effectiveness of rescanning in pencil beam scanned proton therapy for mobile tumours

Stefanie Bertschi[1,2,*], **Miriam Krieger**[1], **Damien C Weber**[1,3,4], **Antony J Lomax**[1,2] and **Steven van de Water**[1,5]

[1] Paul Scherrer Institute, Center for Proton Therapy, Villigen PSI, Switzerland
[2] ETH Zürich, Department of Physics, Zürich, Switzerland
[3] Department of Radiation Oncology, Inselspital, Bern University Hospital, University of Bern, Switzerland
[4] University Hospital of Zürich, Department of Radiation Oncology, Zürich, Switzerland
[5] Department of Radiation Oncology, Amsterdam UMC, Vrije Universiteit Amsterdam, Cancer Center Amsterdam, Amsterdam, The Netherlands
[*] Author to whom any correspondence should be addressed.

E-mail: stefanie.seraina@gmail.com

Keywords: proton therapy, PBS, motion mitigation, rescanning, spot reduction, energy-layer reduction, liver and lung cancer

Supplementary material for this article is available online

Abstract

Objective. In pencil beam scanning proton therapy, individually calculated and positioned proton pencil beams, also referred to as 'spots', are used to achieve a highly conformal dose distributions to the target. Recent work has shown that this number of spots can be substantially reduced, resulting in shorter delivery times without compromising dosimetric plan quality. However, the sensitivity of spot-reduced plans to tumour motion is unclear. Although previous work has shown that spot-reduced plans are slightly more sensitive to small positioning inaccuracies of the individual pencil beams, the resulting shorter delivery times may allow for more rescanning. The aim of this study was to assess the impact of tumour motion and the effectiveness of 3D volumetric rescanning for spot-reduced treatment plans. *Approach.* Three liver and two lung cancer patients with non-negligible motion amplitudes were analysed. Conventional and probabilistic internal target volume definitions were used for planning considering single or multiple breathing cycles respectively. For each patient, one clinical and two spot-reduced treatment plans were created using identical field geometries. 4D dynamic dose calculations were then performed and resulting target coverage (V95%), dose homogeneity (D5%–D95%) and hot spots (D2%) evaluated for 1–25 rescans. *Main results*. Over all patients investigated, spot reduction reduced the number of spots by 91% in comparison to the clinical plan, reducing field delivery times by approximately 50%. This reduction, together with the substantially increased dose per spot resulting from the spot reduction process, allowed for more rescans in the same amount of time as for clinical plans and typically improved dosimetric parameters, in some cases to values better than the reference static (3D calculated) plans. However, spot-reduced plans had an increased possibility of interference with the breathing cycle, especially for simulations of perfectly repeatable breathing. *Significance.* For the patients analysed in this study, spot-reduced plans were found to be a valuable option to increase the efficiency of 3D volumetric rescanning for motion mitigation, if attention is paid to possible interference patterns.

1. Introduction

Plan optimisation for pencil beam scanned (PBS) proton therapy is a highly degenerate problem, with very different patterns and distributions of individually optimised beam weights resulting in very similar dose distributions. For instance, a recent study by Van de Water *et al* (2020) showed that, for a nasal cavity case, the number of delivered Bragg peaks (spots) could be greatly reduced during the optimisation process, resulting in

substantially reduced delivery times, whilst simultaneously preserving plan quality. Such reduced delivery times could be of great benefit clinically and economically, as both patient comfort and patient throughput could be increased, reducing treatment costs potentially, thus allowing proton therapy to be offered to more patients (Schippers *et al* 2018, Bortfeld *et al* 2021). Despite these first promising results however, there are a number of clinical settings where the effectiveness of spot reduction still needs to be investigated and evaluated.

One such is the treatment of mobile tumours. The use of PBS for the treatment of mobile tumours is typically more challenging than the passive scattering approach, because of the dynamic delivery of the dose to a moving target (Paganetti 2018). If motion is not being taken into account during planning and delivery, interplay effects are likely to occur, meaning that spots are not delivered at the location in the target where they were planned, which might result in severe over- and underdosages (Phillips *et al* 1992, Bert *et al* 2008). To minimise such effects, motion mitigation techniques (Keall *et al* 2006), such as gating (De Ruysscher *et al* 2015), breath-hold (Dueck *et al* 2016, Hoppe *et al* 2017), rescanning (Knopf *et al* 2011), tracking (Bert *et al* 2007) or a combination of several techniques can be applied.

At PSI, rescanning has been routinely used for several years (Lim *et al* 2020, Gut *et al* 2021). Rescanning has the advantage of being applied during free-breathing with no need of monitoring the tumour or the breathing pattern of the patient online (Krieger *et al* 2020). With this approach, the target's radiation delivery is scanned several times, each time delivering only a portion of the full fraction dose, in order to achieve a statistical averaging of positioning errors, therefore minimizing the risk of large dose discrepancies (Knopf *et al* 2011). On the other hand, rescanning inevitably increases the delivery time (Bernatowicz *et al* 2013) simply due to the fact that many Bragg peak positions need to be visited multiple times during the scanning process. Given the substantially reduced delivery times, spot reduction could therefore also be an interesting technique for rescanning. On the other hand, spot-reduced plans have been found to be more sensitive to small positioning inaccuracies between the pencil beams and could thus be much more sensitive to the interplay effect than conventional PBS plans (Van de Water *et al* 2020). As such, the aim of this study was to assess the impact of tumour motion and the effectiveness of 3D volumetric rescanning for spot-reduced proton treatment plans.

2. Methods and materials

2.1. Patient data

2.1.1. Patient geometries

Three liver cancer patients with clinical target volumes (CTV) of 264 cm^3, 403 cm^3 and 122 cm^3, and two lung cancer patients (CTVs 19 cm^3 and 142 cm^3) have been included in this study. Four cases (all liver cases and lung case 1) were extracted from our PSI plan database, whilst lung case 2 was retrieved from the Cancer Imaging Archive (Roman *et al* 2012, Balik *et al* 2013, Clark *et al* 2013, Hugo *et al* 2016, Hugo *et al* 2017). The liver without the CTV and the ipsilateral lung without the CTV were considered as organs at risk (OARs). All patient geometries are shown on full-exhale CT's in figure 1.

2.1.2. Motion

For modelling motion, in this study we have used data extracted from 4DMRI of healthy volunteers, rather than 4DCT. 4DMRI has the advantage of providing motion information for multiple breathing cycles and, due to being acquired in the sagittal or lateral plane (so parallel to the predominant axis of motion), can also reduce motion artefacts that are often present in 4DCT data sets. From this data, multiple simulated 4DCT data sets (4DCT(MRI)) can be generated for each patient using methods described in detail in Boye *et al* (2013). In short, motion vectors are extracted from the 4DMRI data and combined with a full exhale, single phase 3DCT for each patient, using B-spline based deformable image registration in Plastimatch (Krieger *et al* 2018, Krieger *et al* 2020).

For this study, motions extracted from the same multi-breath-cycle 4DMRI of a healthy volunteer has been used for all liver cases. This consisted of 10 full breathing cycles, acquired with a temporal resolution of 0.5 s and a total acquisition time of 200 s. Motions were transferred to each liver case by first matching the liver of the MRI acquisition (healthy volunteer) to each case, and then extracting the motion at each point to warp the liver of the single phase CT. For all liver cases, just the first cycle of this data was used to generate a single 4DCT(MRI) for each case, which consisted of 20 motion states with a total duration of 10 s. In addition however, for liver case 2, multiple 4DCT(MRI) data sets were generated, one for each of the 10 breathing cycles in the full 4DMRI acquisition.

For the lung cases, a different acquired motion pattern, but also extracted from the 4DMRI of a healthy volunteer, was used, which consisted of 63 breathing cycles, each with a temporal resolution of 0.8 s and which led to a total acquisition time of 450 s. As with the liver cases, single cycle 4DCT(MRI)s were generated for both lungs consisting of 9 motion states with a period of 7.2 s. Additionally, a multi-cycle 4DCT(MRI) data set was

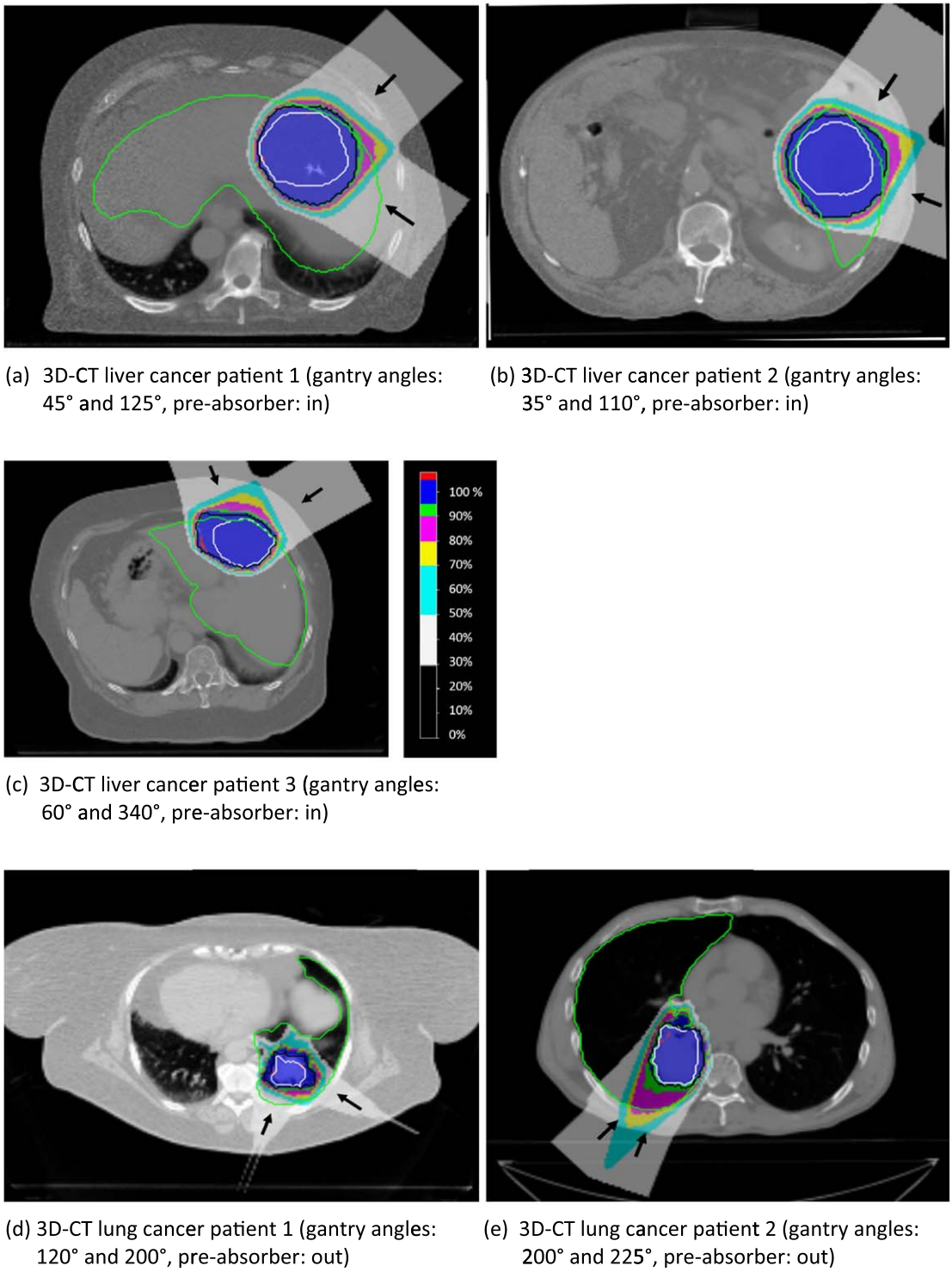

(a) 3D-CT liver cancer patient 1 (gantry angles: 45° and 125°, pre-absorber: in)

(b) 3D-CT liver cancer patient 2 (gantry angles: 35° and 110°, pre-absorber: in)

(c) 3D-CT liver cancer patient 3 (gantry angles: 60° and 340°, pre-absorber: in)

(d) 3D-CT lung cancer patient 1 (gantry angles: 120° and 200°, pre-absorber: out)

(e) 3D-CT lung cancer patient 2 (gantry angles: 200° and 225°, pre-absorber: out)

Figure 1. Planned dose distributions shown on full exhale 3D-CTs for three liver and two lung cancer patients with the CTV (white), the OARs (green) and the target volumes used for planning (black). The arrows indicate the chosen beam angles.

also generated for lung case 2 using all the motion data. Both multi-cycle data sets (one each for liver and lung) were used to additionally investigate the effects of irregular motion on both conventional and spot-reduced plans.

2.2. Treatment planning

2.2.1. Target definition

For the single cycle data sets, conventional internal target volumes (ITV) (MD:ICRU 2007) have been created by unifying the CTVs of all motion states within each patient's 4DCT (MRI). In contrast, for the two multiple-cycle

4D data sets, a probabilistic ITV has been defined, as described by Krieger *et al* (2020). For this, a conventional ITV is defined for each individual breathing cycle, with the resulting ITV masks being then used to create a final probabilistic ITV by selecting all voxels that are included within at least this defined percentage of the breathing cycle. In Krieger *et al* (2020) it was shown that a selection probability of 50% is an adequate compromise between target coverage and dose to OARs, and that is the level adopted here.

For both the conventional and the probabilistic ITVs, the single CTs of all considered motion states were combined to generate a synthetic planning CT. For this, the Hounsfield units (HU) for voxels outside the ITV contour were averaged over all motion states, while for voxels inside the ITV, a maximum-intensity-projection approach was used (Botas *et al* 2018). Additional uncertainties in proton range, patient positioning or non-motion related anatomical changes have not been considered in this study.

2.2.2. Clinical treatment plans

All clinical treatment plans were generated using 'PSI plan', the clinical in-house treatment planning system for gantry 2 at PSI (Weber *et al* 2005). In this, all possible spots contributing useful dose to the defined target volume are first identified, after which the dose for each spot is calculated and optimised using a ray-casting algorithm (Lomax 1999, Schaffner *et al* 1999). Two field plans have been calculated for all plans, and a prescription dose of 2 Gy_{RBE} assumed (RBE $=$ 1.1). For superficial targets, a 42 mm pre-absorber was used. A 4 mm rectangular spot placement grid orthogonal to the beam direction and 2.5 mm in (water-equivalent) depth was used and each field was optimised using the single field, uniform dose (SFUD) approach to ensure that each plan delivered as homogenous dose as possible to the target volume (Harding *et al* 2014, Gorgisyan *et al* 2019). Identical planning geometries and parameters have been used for plans calculated using either conventional or probabilistic ITV's. Field arrangements and specifications for all cases are shown in figure 1.

2.2.3. Spot-reduced treatment plans

Corresponding spot-reduced treatment plans were generated with the spot reduction treatment planning system developed by Van de Water *et al* (2020). This treatment planning system is based on the open-source software for radiation treatment planning 'matRad' (Wieser *et al* 2017), which was extended with the iterative 'pencil beam resampling' optimisation technique to reduce the number of spots (Van de Water *et al* 2015). Compared with the conventional treatment planning system, not all possible candidate spots are optimised at once, with only a random sub-sample being included in each iteration. The dose is then calculated and optimised for this sub-sample. Prioritised multi-criteria optimisation is used, meaning that objectives are optimised according to a user-defined order, while constraining the achieved values of objectives with a higher priority. Dose optimisation is followed by repeated exclusion of low-weighted spots and re-optimisation of spot weights, until further spot reduction would result in a worsening of dosimetric plan quality. This whole procedure is repeated by adding another random subsample of spots to the remaining optimised spots from the previous iteration, until all objectives are achieved or none of the objectives improves by more than 3%. In this study, we used a sample size of 5000 randomly selected spots in each iteration.

To be consistent with the clinical treatment plans, the same field arrangement (i.e. isocentre, gantry angles, pre-absorber, spot spacing and energy layer separation) and fraction dose was used for the spot-reduced plans. Additional target dose homogeneity objectives were included for each beam individually during multi-field optimisation to also achieve a similar uniformity of dose across the target for each field as in the clinical plans. In addition, the planning system has the additional option to also reduce the number of energy layers, after which spot reduction is performed for the remaining energy layers. As such, plans with (referred to as 'energy-layer-reduced plans') and without this option (referred to as 'spot-reduced-plans') were generated for all patients.

2.3. 4D simulations

2.3.1. 4D dynamic dose calculations.

The effect of motion for all plans was assessed using the deformable dose grid 4D dynamic dose calculation combined with estimates of timing of the delivery for each spot based on the known delivery characteristics of the PSI gantry 2. We assumed dead times of 80 ms between energy layers, 3 ms for lateral spot adjustments and beam intensities ranging between 1.4 and 2.9 Giga-protons s^{-1} for energies of 73–299 MeV (Zhang *et al* 2018, Van de Water *et al* 2019). For a full description of this approach, see Boye *et al* (2013) and Krieger *et al* (2018), Krieger *et al* (2020).

2.3.2. Rescanning

At PSI, rescanning has been used for several years to treat mobile tumours (Lim *et al* 2020, Gut *et al* 2021). Specifically, a hybrid method between scaled and iso-layered rescanning is used (Zenklusen *et al* 2010). In this, where possible, the spot dose is divided into n equal parts, where n is the number of rescans. In the case that the weight of a particular spot is too low to meet the minimum deliverable spot weight however, the number of

rescans is reduced until the partial spot is deliverable. In addition, we use full 3D volumetric rescanning, in which rescanning is not applied to individual energy layers, but over the whole volume for each rescan (Bernatowicz *et al* 2013, Zhang *et al* 2016), together with energy meandering, whereby the direction of energy change (high-to-low or low-to-high) is alternated between each volumetric sub-scan (Actis *et al* 2018). This has also been used in all simulations in this work. Finally, the mitigating effects of 1 (i.e. no rescanning) to 25 rescans have been simulated for all plans and cases.

2.3.3. Simulation scenarios

Simulations were performed by varying three characteristics: (1) the treatment plan, (2) the motion pattern (with corresponding ITV definition) and (3) the starting phase.

For each patient, clinical, spot-reduced and energy-layer-reduced treatment plans were generated using the corresponding single-cycle 4DCT(MRI) and conventional ITV. Additionally, for liver case 2 and lung case 2, plans were also generated on multi-cycle 4DCT(MRI) using the probabilistic ITV. As for all cases the duration of the single cycle breathing pattern is shorter than the time to deliver a field, it was extended by repeating the same breathing pattern multiple times, thus simulating perfectly repeatable breathing. In addition, since the phase of the breathing cycle when starting the delivery is usually unknown, multiple 4D calculations were performed for different combinations of starting phase within this cycle for each field. As such, a total of around 138 000 4D dynamic dose calculations have been performed in this study. A detailed overview of all the simulations performed, can be found in table 1.

2.4. Analysis

2.4.1. Dosimetric analysis

All static plans have been analysed by evaluating ITV coverage in terms of V95%, D5%–D95% (dose homogeneity) and dose hot spots (D2%), with these values being used as references for the subsequent analysis of the 4D calculations. For the evaluation and comparison of the 4D plans, the corresponding values were calculated considering the CTV instead of the ITV. The OAR were defined to be the liver or ipsilateral lung, excluding the CTV, for which we calculated the mean doses for all plans and 4D dynamic dose calculations.

3. Results

3.1. Treatment planning characteristics

CTV, conventional and probabilistic ITV volumes, together with the number of spots and energy layers for each plan, are shown in tables 2 and 3. Also shown in the tables are V95%, D5%–D95% and D2% for the conventional ITV as calculated for the static (reference) plan. Of note, the use of multiple breathing cycles for defining the probabilistic ITV's reduced ITV volumes on average by 14% compared to the conventional ITVs for the two cases where these were calculated. Compared to the clinical plan, spot reduction reduced the number of spots by on average 91% and the number of energy layers by on average 7% (between 5% and 10%). Even more spots could be removed for the energy-layer-reduced plans, with the number of energy layers being decreased by between 21% and 61%. V95%, D5%–D95% and D2% to the ITV for both were very comparable to the clinical plans.

3.2. One breathing cycle—conventional ITV

3.2.1. Liver cancer patients

Figure 2 shows the results of the simulations with a single repeated breathing cycle using the conventional ITV definition for the three liver cancer patients, with solid lines showing the median over all simulations, and the 5–95th percentile of their variation due to differing starting phases shown as the shaded bands. V95%, D5%–D95% and D2% to the CTV are shown as a function of delivery time (total time to deliver all fields without taking into account gantry rotations), whilst the mean doses to the healthy liver are shown as a function of the number of rescans.

For liver cancer patient 1, the time needed to deliver one scan (i.e. no motion mitigation) was reduced from 105 s for the clinical plan to 55 and 49 s for the spot-reduced and the energy-layer-reduced treatment plans respectively, whilst the treatment times for 25 rescans were reduced from 519 to 342 and 200 s. Since spot and energy-layer-reduced plans were delivered in shorter times than the clinical plan, more rescans could be performed in the same amount of time, so that dose to the CTV recovered to the values of the static plan more quickly. For instance, the CTV V95% median value increased above 95% after 252, 90 and 68 s for the clinical, the spot-reduced and the energy-layer-reduced treatment plan respectively. In addition, the mean dose to the healthy liver was comparable for all plans.

Table 1. Summary of all 4D dynamic dose calculations performed. For each patient with its corresponding target definition listed in the first column, 4D dynamic dose calculations were performed for all possible combinations of each motion state in the first breathing cycle (for two fields), for all number of rescans and for each treatment plan (i.e. clinical, spot-reduced and energy-layer-reduced). The resulting total numbers of 4D dynamic dose calculations are shown in the last column.

Patients (target definition)	All possible combinations of motion states in first breathing cycle (for two fields)	Number of rescans	Treatment plans	Number of 4D dynamic dose calculations
3 liver cancer patients (conventional ITV)	$20 \times 20 = 400$	25	3 (i.e. clinical, spot-reduced, energy-layer-reduced)	90 000
1 liver cancer patient (probabilistic ITV)	$20 \times 20 = 400$	25	3 (i.e. clinical, spot-reduced, energy-layer-reduced)	30 000
2 lung cancer patients (conventional ITV)	$9 \times 9 = 81$	25	3 (i.e. clinical, spot-reduced, energy-layer-reduced)	12 150
1 lung cancer patient (probabilistic ITV)	$9 \times 9 = 81$	25	3 (i.e. clinical, spot-reduced, energy-layer-reduced)	6075
			Total number of 4D dynamic dose calculations	138 225

Table 2. Overview of all patients planned on the conventional ITV with one breathing cycle. The last three columns show the ITV values for the static case.

	CTV size [cm^3]	ITV size [cm^3]	Treatment planning scenario	Number of spots (reduction compared to clinical plan)	Number of energy layers (reduction compared to clinical plan)	ITV V95%	ITV D5%-D95%	ITV D2%
Liver	263.9	416.2	Clinical plan	15746	106	96.3	9.5	105.7
Patient 1			Spot-reduced	1238 (−92%)	97 (−9%)	98.6	5.3	104
			E-layer-red.	1008 (−94%)	37 (−61%)	98.6	5.2	104.1
Liver	403.4	574.5	Clinical plan	31477	99	99.9	3.4	102.8
Patient 2			Spot-reduced	1779 (−94%)	91 (−8%)	99.9	4.6	104.4
			E-layer-red.	1474 (−95%)	71 (−33%)	99.8	4.5	104.4
Liver	122.2	203.5	Clinical plan	13144	72	98.6	5.6	104.1
Patient 3			Spot-reduced	953 (−93%)	65 (−10%)	99	4.2	103.9
			E-layer-red.	865 (−93%)	30 (−58%)	99.2	4.1	104
Lung	18.8	74.2	Clinical plan	3183	43	100	6.2	105.4
Patient 1			Spot-reduced	496 (−84%)	40 (−7%)	99.7	4.6	104.6
			E-layer-red.	588 (−82%)	24 (−44%)	99.9	4.8	104.8
Lung	141.9	234.4	Clinical plan	11769	65	99.7	7.6	106.4
Patient 2			Spot-reduced	1392 (−88%)	62 (−5%)	99.2	6.7	106
			E-layer-red.	1114 (−91%)	43 (−34%)	99.3	6.4	105.7

Table 3. Overview of the patients planned on the probabilistic ITV with multiple breathing cycles. The last three columns show the ITV values for the static case.

	CTV size [cm^3]	ITV size (prob.) [cm^3]	Treatment planning scenario	Number of spots (reduction compared to clinical plan)	Number of energy layers (reduction compared to clinical plan)	ITV V95%	ITV D5%–D95%	ITV D2%
Liver	403.4	534.1	Clinical plan	30793	98	97.7	4.7	102.9
Patient 2			Spot-reduced	1576 (−95%)	93 (−5%)	97.7	6.3	104.5
			E-layer-red.	1387 (−95%)	42 (−57%)	97.8	5.8	104.2
Lung	141.9	187.8	Clinical plan	12152	67	99.6	7.5	106
Patient 2			Spot-reduced	1492 (−88%)	63 (−6%)	99.2	6.3	105.7
			E-layer-red.	1151 (−91%)	53 (−21%)	99.3	6.4	105.6

Similar results were observed for liver cancer patients 2 and 3. Treatment times were again reduced substantially for the spot and energy-layer-reduced treatment plans, so that acceptable values were reached more quickly for all parameters for all patients. The mean dose to the liver excluding the CTV was also comparable for all plans and all patients. Additionally, it can be seen for liver cancer patients 2 and 3 that the median of D5%–D95% to the CTV for the clinical plan only approached but did not reach the value of the static plan, while the median D5%–D95% for the spot- and energy-layer-reduced treatment plans improved to beyond the static values. Rescanning for the spot and energy-layer-reduced treatment plans was generally therefore not only more efficient, but also typically more effective at mitigating motion effects. However, the best results were not necessarily found for the largest number of rescans, as the metrics did not monotonically improve with increasing numbers of rescans for any of the cases. That is, fluctuations in all values were observed, particularly for the spot- and energy-reduced plans. For instance, for D2% for liver case 3, the spot-reduced plan reaches a minimum for delivery times of just above 100 s but increases again for the longer treatment times as the number of rescans increases. Similar effects have already been seen in studies by Zenklusen *et al* (2010), Bernatowicz *et al* (2013), Zhang *et al* (2016).

3.2.2. Lung cancer patients

Figure 3 shows the results for the single repeated breathing cycle using the conventional ITV definition for the two lung cancer patients. Note that the target of lung cancer patient 1 was considerably smaller and needed therefore fewer spots than all other targets (table 2). This is reflected in the treatment times for this case, which are short even for the clinical plan, meaning that relative differences in efficiency between the plans was less pronounced. As the target of lung cancer patient 2 was considerably larger than for lung cancer patient 1, a more substantial reduction in delivery times and improvement in effectiveness (i.e. the ability to restore planned dose values for a certain number of rescans) of the spot and the energy-layer-reduced plans was however observed. As

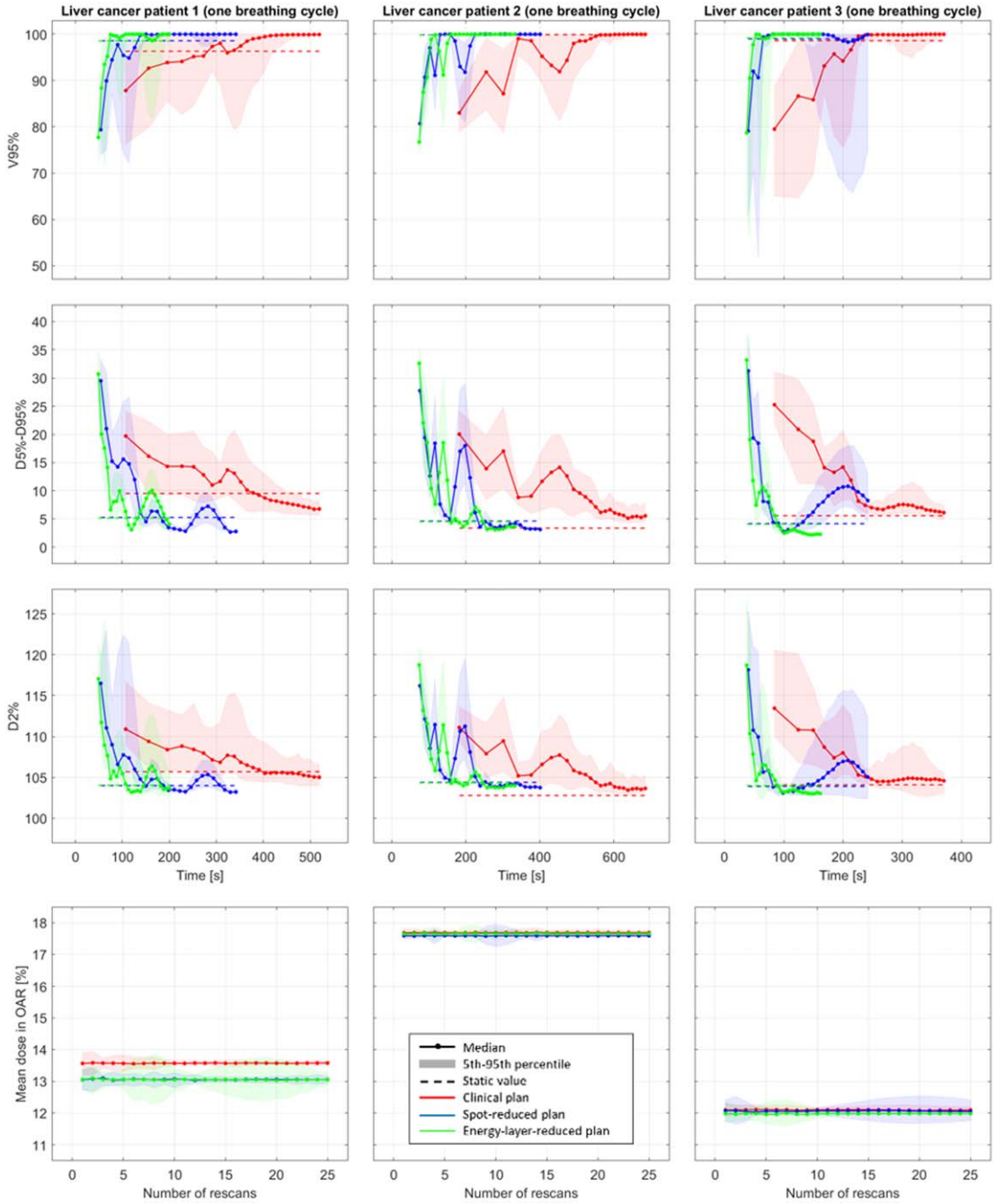

Figure 2. Liver cancer patients: Band plots of CTV V95%, CTV D5%–D95% and CTV D2% shown as a function of the total delivery time with the markers indicating the number of rescans ranging from 1 (i.e. no motion mitigation) up to 25 rescans. The mean dose to the liver without the target is shown as a function of the number of rescans. One breathing cycle and the conventional ITV were used for planning for the clinical, the spot-reduced and the energy-layer-reduced treatment plans.

with the liver cases, fluctuations in the dosimetric values as a function of the number of rescans is observed for the spot- and energy-layer-reduced plans, particularly for small numbers of rescans (shorter delivery times) whereas a much smoother response is observed for the clinical plans. Finally, the integral dose delivered to ipsilateral lung tissue, excluding the target volume, was comparable for all plans for both patients.

3.3. Multiple breathing cycles—probabilistic ITV

For two cases, one liver and one lung, the same simulations have been performed using non-repeated, and more clinically plausible, motion patterns as described in section 2.1 above. Motion patterns of the CTV for the two cases are shown in figure 4 and consist of 10 and 63 full breathing cycles for the liver and lung cases respectively. Results for all simulations for these two cases are shown in figure 5. Although some fluctuations in the dosimetric values to the CTV are still observed (figure 5), particularly for the liver case, these are generally less pronounced than for the repeated motions. Nevertheless, for more than 4 rescans, the median of V95% was

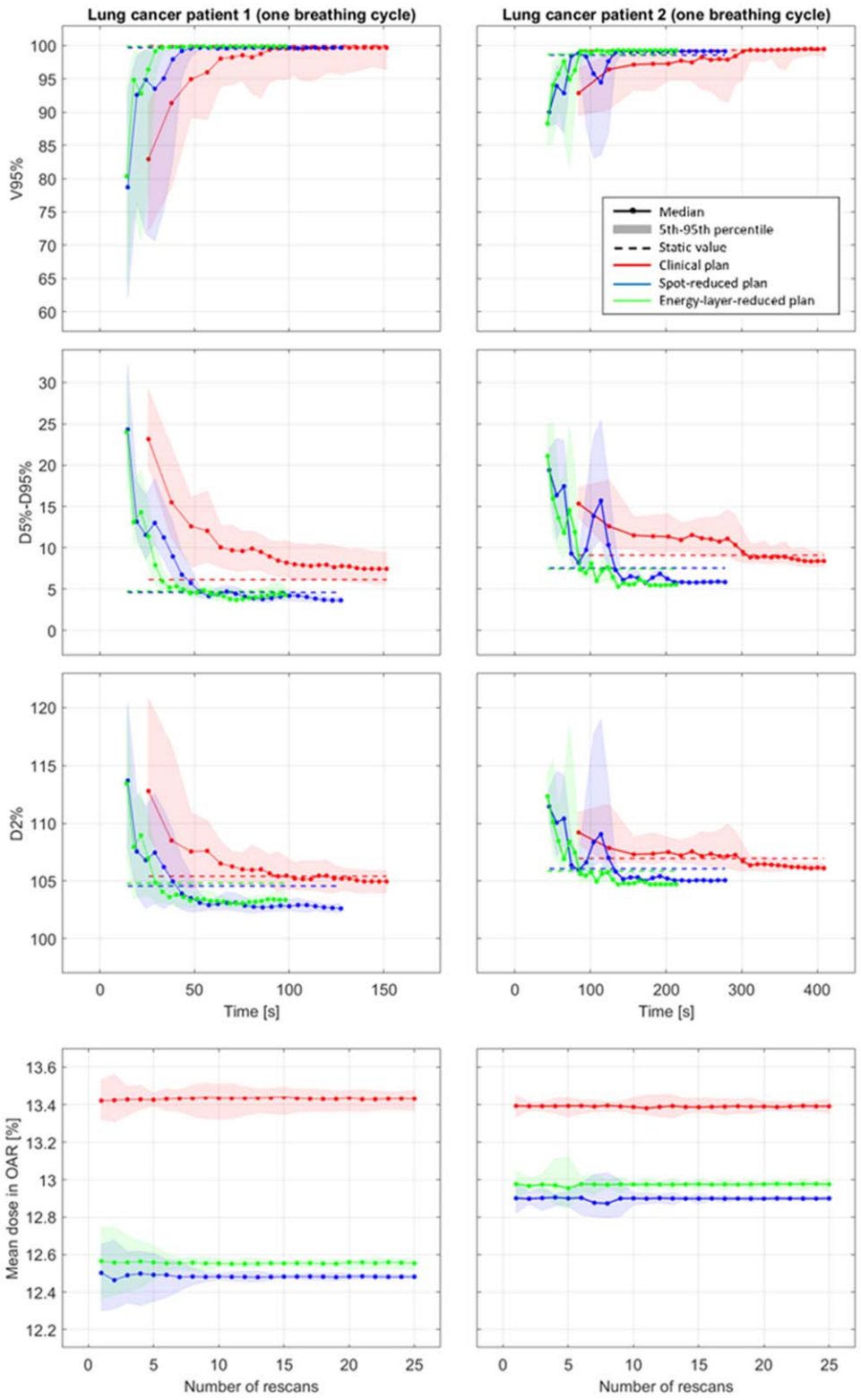

Figure 3. Lung cancer patients: band plots of CTV V95%, CTV D5%-D95% and CTV D2% shown as a function of the total delivery time with the markers indicating the number of rescans ranging from 1 (i.e. no motion mitigation) up to 25 rescans. The mean dose to the ipsilateral lung without the target is shown as a function of the number of rescans. One breathing cycle and the conventional ITV were used for planning for the clinical, the spot-reduced and the energy-layer-reduced treatment plans.

always higher than 93.6% for both the spot and the energy-layer-reduced plans. In contrast, the variation of the CTV dosimetry metrics for the lung case are more predictable and once again show the faster convergence for the spot- and energy-reduced plans to values close to the static cases than for the clinical plan.

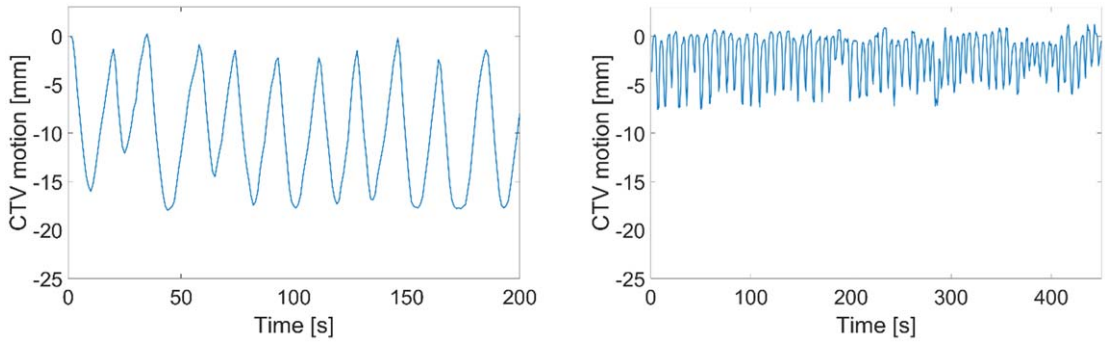

Figure 4. CTV motion (mean motion of all voxels inside CTV) of liver cancer patient 2 (left) and of lung cancer patient 2 (right) in superior-inferior direction. The motion pattern on the left is represented by 10 full breathing cycles, with a temporal resolution of 0.5 s and a total acquisition time of 200 s. The motion pattern on the right consisted of 63 breathing cycles, acquired with a temporal resolution of 0.8 s and a total acquisition time of 450 s.

4. Discussion

In this study, we have investigated the impact of motion on spot-reduced treatment plans for PBS proton therapy, and whether 3D volumetric rescanning is an effective motion mitigation approach for such plans. In total, more than 138 000 4D dynamic dose calculations have been performed using one or multiple breathing cycles, and target coverage (V95%), dose homogeneity (D5%-D95%) and hot spots (D2%) in the CTV evaluated for up to 25 rescans.

The number of spots was reduced by 91% on average for both the spot and the energy-layer-reduced treatment plans, while the number of energy layers was reduced by 7% for the spot-reduced and by 46% for the energy-layer-reduced treatment plans. As such, delivery time could be shortened by approximately 40% and 50% for the spot- and energy-layer-reduced treatment plans respectively when compared to the clinical plan.

That delivery times are not reduced further, is due to the fact that the number of protons that need to be delivered per field remains more or less constant, independent of the number of spots in the field. Thus, the total beam-on time per field is only marginally affected by spot reduction, with the major effect of spot- and energy-layer-reduction being to reduce the total dead-time (i.e. the time to move from spot-to-spot and to change the energy) per field. On the other hand, although not investigated here, the fewer, but consequently much higher weighted spots resulting from spot reduction would allow for the use of higher beam intensities to shorten the treatment time further than reported here (Maradia *et al* 2021, Maradia *et al* 2022). The additional benefit of this is currently under investigation.

Our simulations have shown however, that in addition to reducing treatment time, spot- and energy-layer-reduced treatment plans could also be more efficient for rescanning, by recovering acceptable target coverage and homogeneity in shorter times than for a typical clinical plan. Although the results were very similar for the spot and energy-layer-reduced treatment plans, especially in contrast to the clinical plans, the energy-layer-reduced plans were generally the more efficient, due to the additional advantage of reducing the number of energy level changes. Importantly however, all simulations here have been performed using the delivery dynamics of Gantry 2 at PSI, which has energy switching times of the order of 100 ms for 5 mm WER changes. This is considerably faster than most commercial machines, and therefore we would expect the advantage of energy-layer-reduced plans to be even more if applied on machines with slower layer switching times.

In spot and energy-layer-reduced treatment plans, most of the spots could be rescanned the desired number of times, thus making rescanning more effective. On the other hand, this makes the effectiveness of rescanning fluctuate as a function of the number of rescans. Rescanning relies on achieving a statistical smearing of hot and cold spots, under the assumption that these will occur in different places within the target in each individual sub-scan. However, this will only be the case if the start of each sub-scan starts at a different point of the breathing cycle. This may not be the case for the spot and energy-layer-reduced plans however, where, due to their substantially higher weights, all spots can be rescanned the required number of times (even for the highest rescan factor investigated here (25) around 90% of spots can be rescanned the full 25 times). Consequently, each sub-scan will take approximately the same amount of time to deliver, leading to the possibility of synchronization of the start of each sub-scan with the same phase of the (repeated) breathing cycle. In contrast, due to the large number of low weighted spots in the clinical plans, the number of spots that will be fully rescanned gradually reduces as the rescan factor increases, with only about 10% of spots being fully rescanned for a rescan factor of 25. As such, the time per sub-scan gradually decreases throughout the rescanning process, helping break possible interferences between the scanning and motion timelines. Such effects are clearly seen for all liver and lung cases

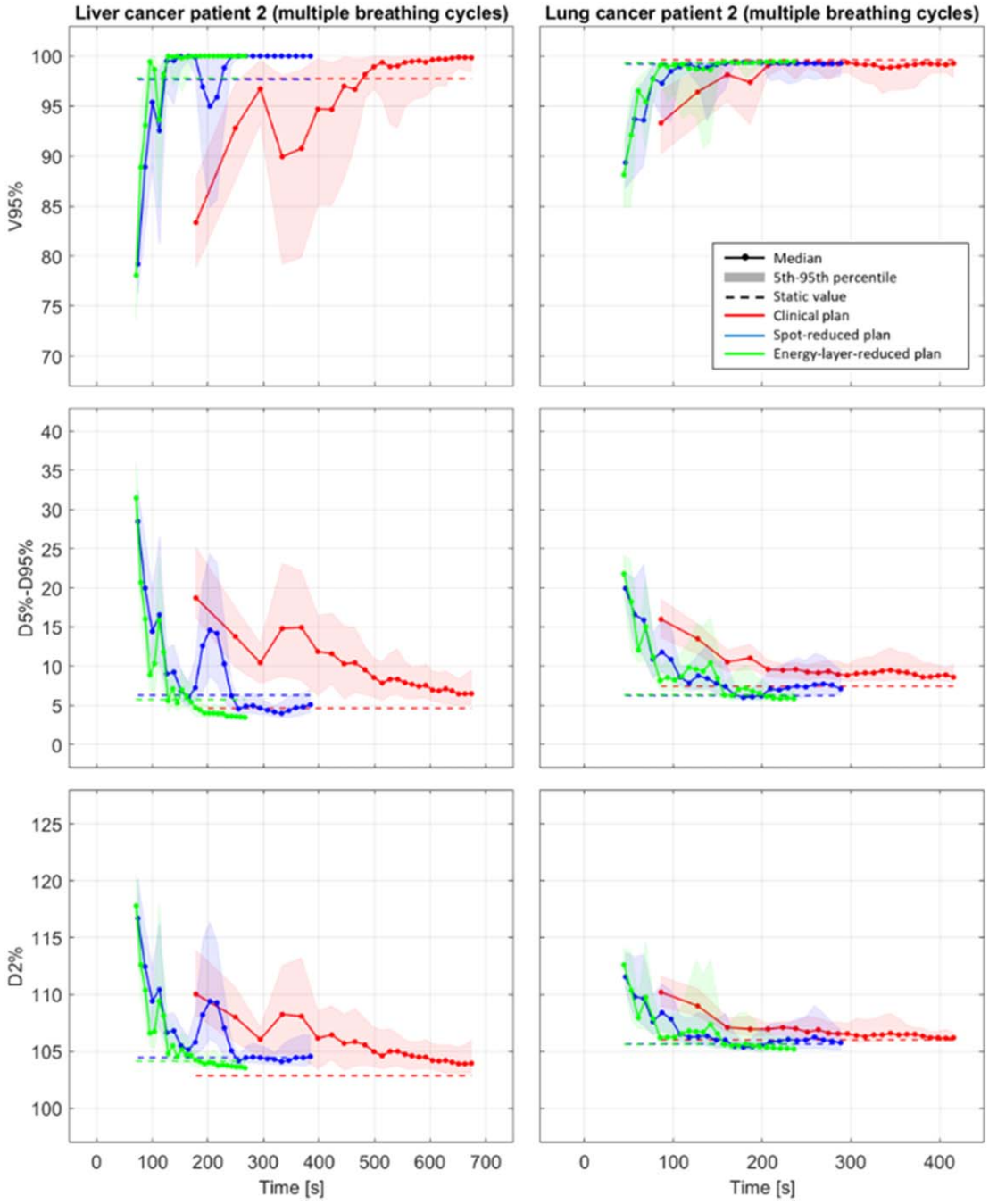

Figure 5. Band plots of CTV V95%, CTV D5%–D95% and CTV D2% are shown as a function of the total delivery time with the markers indicating the number of rescans ranging from 1 (i.e. no motion mitigation) up to 25 rescans for liver cancer patient 2 and lung cancer patient 2. Multiple breathing cycles and the probabilistic ITV with a threshold of 50% were used for planning for the clinical, the spot-reduced and the energy-layer-reduced treatment plans.

when the perfectly repeatable breathing patterns were used, but were somewhat reduced for the irregular breathing patterns, which are anyway clinically more plausible. Nevertheless, it maybe be necessary to introduce some additional measures to mitigate this effect for spot- and energy-layer-reduced plans in practice, such as introducing random delays, changing the order or speed of scanning or using breath-sampled rescanning techniques as suggested by Furukawa *et al* Seco *et al* and Engwall *et al* respectively (Furukawa *et al* 2007, Seco *et al* 2009, Engwall *et al* 2018a, 2018b).

Finally, our 'one breathing cycle—conventional ITV' approach can be considered a typical clinical approach and is largely in line with international guidelines and recommendations of the ICRU (ICRU 2007), AAPM (Li *et al* 2022) and PTCOG (Chang *et al* 2017). Although 4DCT(MRI) data were used as input, when only considering a single breathing cycle, these can easily be replaced by more conventional 4DCT scans. There are multiple techniques still under investigation to handle motion irregularities effectively (Engwall *et al*

2018a, 2018b). In this study, we considered the 'probabilistic ITV', an in-house developed technique, for which it was found that the definition of the ITV has direct consequences on the target coverage and the dose to healthy tissue in the presence of motion irregularities (Krieger *et al* 2020). It was shown that a threshold of 50% is an adequate compromise between target coverage and dose to organs at risk for the lung cancer patients used in this thesis. Nevertheless, it could be that a different threshold is more favourable for the liver cancer patients. Alternatively, it could also be investigated whether 4D robust optimization is able to mitigate those effects of motion irregularities (Knopf *et al* 2022). Such an investigation however was out of the scope of this work.

5. Conclusion

For the patients analysed in this study, spot and energy-layer-reduced treatment plans have been found to be a potentially valuable option for more efficient and effective treatment delivery in terms of target coverage, homogeneity and severity of hot spots, when using 3D volumetric rescanning for treating liver and lung tumours. However, the regular delivery pattern of spot and energy-layer-reduced plans increased the possibility of interference, especially for perfectly repeatable breathing patterns. For clinically typical free breathing patterns, which include natural breathing irregularities, the impact of this effect however is somewhat mitigated.

Acknowledgments

SvdW was supported by the EU-H2020 project 'INSPIRE' (INfraStructure in Proton International REsearch; Grant ID: 730983). MK received funding by the Swiss National Science Foundation (SNF) Grant No. 320030_163330/1. The authors would like to thank Dr Ye Zhang for sharing imaging data sets.

ORCID iDs

Stefanie Bertschi https://orcid.org/0000-0001-5958-8193
Miriam Krieger https://orcid.org/0000-0002-1914-1220

References

Actis O, Mayor A, Meer D and Weber D C 2018 Precise beam delivery for proton therapy with dynamic energy modulation *J. Phys. Conf. Ser.* **1067** 092002

Balik S *et al* 2013 Evaluation of 4-dimensional computed tomography to 4-dimensionalcone-beam computed tomography deformable image registration for lung cancer adaptive radiation therapy *Int. J. Radiat. Oncol.* Biol.* Phys.* **86** 372–9

Bernatowicz K, Lomax A J and Knopf A 2013 Comparative study of layered and volumetric rescanning for different scanning speeds of proton beam in liver patients *Phys. Med. Biol.* **58** 7905–20

Bert C, Grözinger S O and Rietzel E 2008 Quantification of interplay effects of scanned particle beams and moving targets *Phys. Med. Biol.* **53** 2253–65

Bert C, Saito N, Schmidt A, Chaudhri N, Schardt D and Rietzel E 2007 Target motion tracking with a scanned particle beam *Med. Phys.* **34** 4768–71

Bortfeld T R, Fernandez de Viana M and Yan S 2021 The societal impact of ion beam therapy *Z. Med. Phys.* **31** 102–4

Botas P, Grassberger C, Sharp G and Paganetti H 2018 Density overwrites of internal tumor volumes in intensity modulated proton therapy plans for mobile lung tumors *Phys. Med. Biol.* **63** 035023

Boye D, Lomax T and Knopf A 2013 Mapping motion from 4d-mri to 3d-ct for use in 4d dose calculations: A technical feasibility study *Med. Phys.* **40** 061702

Chang J Y *et al* 2017 Consensus guidelines for implementing pencil-beam scanning proton therapy for thoracic malignancies on behalf of the PTCOG thoracic and lymphoma subcommittee *Int. J. Radiat. Oncol.* Biol.* Phys.* **99.1** 41–50

Clark K *et al* 2013 The cancer imaging archive (tcia): maintaining and operating a public information repository *J. digit. imaging* **26** 1045–57

Dueck J, Knopf A-C, Lomax A, Albertini F, Persson G F, Josipovic M, Aznar M, C.Weber D and Af Rosenschöld P M 2016 Robustness of the voluntary breath-hold approach for the treatment of peripheral lung tumors using hypofractionated pencil beam scanning proton therapy *Int. J. Radiat. Oncol.* Biol.* Phys.* **95** 534–41

Engwall E, Fredriksson A and Glimelius L 2018 4D robust optimization including uncertainties in time structures can reduce the interplay effect in proton pencil beam scanning radiation therapy *Med. Phys.* **45.9** 4020–9

Engwall E, Glimelius L and Hynning E 2018 Effectiveness of different rescanning techniques for scanned proton radiotherapy in lung cancer patients *Phys. Med. Biol.* **63** 095006

Furukawa T, Inaniwa T, Sato S, Tomitani T, Minohara S, Noda K and Kanai T 2007 Design study of a raster scanning system for moving target irradiation in heavy-ion radiotherapy *Med. Phys.* **34** 1085–97

Gorgisyan J *et al* 2019 The dosimetric effect of residual breath-hold motion in pencil beam scanned proton therapy–an experimental study *Radiother. Oncol.* **134** 135–42

Gut P, Krieger M, Lomax T, Weber D C and Hrbacek J 2021 Combining rescanning and gating for a time-efficient treatment of mobile tumors using pencil beam scanning proton therapy *Radiother. Oncol.* **160** 82–9

Harding R, Trnkov A P, Weston S, Lilley J, Thompson C, Short S, Loughrey C, Cosgrove V, Lomax A J and Thwaites D 2014 Benchmarking of a treatment planning system for spot scanning proton therapy: comparison and analysis of robustness to setup errors of photon imrt and proton sfud treatment plans of base of skull meningioma *Med. Phys.* **41** 111710

Hoppe B S, Mendenhall N P, Louis D, Li Z and Flampouri S 2017 Comparing breath hold and free breathing during intensity-modulated radiation therapy and proton therapy in patients with mediastinal hodgkin lymphoma *Int. J. Part. Ther.* **3** 492–6
Hugo G D, Weiss E, Sleeman W C, Balik S, Keall P, Lu J and Williamson J 2016 Data from4d lung imaging of nsclc patients *Cancer Imaging Archive* **10** K9
Hugo G D, Weiss E, Sleeman W C, Balik S, Keall P J, Lu J and Williamson J F 2017 A longitudinal four-dimensional computed tomography and cone beam computed tomography dataset for image-guided radiation therapy research in lung cancer *Med. Phys.* **44** 762–71
Keall P J *et al* 2006 The management of respiratory motion in radiation oncology report of aapm task group 76 a *Med. Phys.* **33** 3874–900
Knopf A C *et al* 2022 Clinical necessity of multi-image based (4DMIB) optimization for targets affected by respiratory motion and treated with scanned particle therapy—a comprehensive review *Radiother. Oncol.* **169** 77–85
Knopf A-C, Hong T S and Lomax A 2011 Scanned proton radiotherapy for mobile targets—the effectiveness of rescanning in the context of different treatment planning approaches and for different motion characteristics *Phys. Med. Biol.* **56** 7257
Krieger M, Giger A, Salomir R, Bieri O, Celicanin Z, Cattin P C, Lomax A J, Weber D C and Zhang Y 2020 Impact of internal target volume definition for pencil beam scanned proton treatment planning in the presence of respiratory motion variability for lung cancer: A proof of concept *Radiother. Oncol.* **145** 154–61
Krieger M, Klimpki G, Fattori G, Hrbacek J, Oxley D, Safai S, Weber D C, Lomax A J and Zhang Y 2018 Experimental validation of a deforming grid 4d dose calculation for pbs proton therapy *Phys. Med. Biol.* **63** 055005
Li H *et al* 2022 AAPM task group report 290: respiratory motion management for particle therapy *Med. Phys.* **49.4**
Lim P S, Pica A, Hrbacek J, Bachtiary B, Walser M, Lomax A J and Weber D C 2020 Pencil beam scanning proton therapy for paediatric neuroblastoma with motion mitigation strategy for moving target volumes *Clin. Oncol.* **32.7** 467–76
Lomax A 1999 Intensity modulation methods for proton radiotherapy *Phys. Med. Biol.* **44** 185–205
Maradia V, Giovannelli A C, Meer D, Weber D C, Lomax A J, Schippers J M and Psoroulas S 2022 Increase of the transmission and emittance acceptance through a cyclotron-based proton therapy gantry *Med. Phys.* **49** 2103–92
Maradia V, Meer D, Weber D C, Lomax A J, Schippers J M and Psoroulas S 2021 A new emittance selection system to maximize beam transmission for low-energy beams in cyclotron-based proton therapy facilities with gantry *Med. Phys.* **48** 7613–22
Jones D, Suit H, Kanematsu N, Tatsuzaki H and Tsujii H 2007 ICRU Report 78, Prescribing, Recording, and Reporting Proton-Beam Therapy *ICRU Report* **7** 1–210 https://icru.org/report/prescribing recording-and-reporting-proton-beam-therapy-icru-report-78/
Phillips M H, Pedroni E, Blattmann H, Boehringer T, Coray A and Scheib S 1992 Effects of respiratory motion on dose uniformity with a charged particle scanning method *Phys. Med. Biol.* **37** 223–34
Paganetti H (ed) 2018 Proton Therapy Physics *Proton Therapy Physics* 2nd edn (London: CRC Press) (https://doi.org/10.1201/b22053)
Roman N O, Shepherd W, Mukhopadhyay N, Hugo G D and Weiss E 2012 Interfractional positional variability of fiducial markers and primary tumors in locally advanced non-small-cell lung cancer during audiovisual biofeedback radiotherapy *Int. J. Radiat. Oncol.* Biol.* Phys.* **83** 1566–72
De Ruysscher D, Sterpin E, Haustermans K and Depuydt T 2015 Tumour movement in proton therapy: solutions and remaining questions: a review *Cancers* **7** 1143–53
Schaffner B, Pedroni E and Lomax A 1999 Dose calculation models for proton treatment planning using a dynamic beam delivery system: an attempt to include density heterogeneity effects in the analytical dose calculation *Phys. Med. Biol.* **44** 27–41
Schippers J M, Lomax A, Garonna A and Parodi K 2018 Can technological improvements reduce the cost of proton radiation therapy? *Semin. Radiat. Oncol.* **28** 150–9
Seco J, Robertson D, Trofimov A and Paganetti H 2009 Breathing interplay effects during proton beam scanning: simulation and statistical analysis *Phys. Med. Biol.* **54** N283–94
Van de Water S, Belosi M F, Albertini F, Winterhalter C, Weber D C and Lomax A J 2020 Shortening delivery times for intensity-modulated proton therapy by reducing the number of pro-ton spots: an experimental verification *Phys. Med. Biol.* **65** 095008
Van de Water S, Kooy H M, Heijmen B J and Hoogeman M S 2015 Shortening delivery times of intensity modulated proton therapy by reducing proton energy layers during treatment plan optimization *Int. J. Radiat. Oncol.* Biol.* Phys.* **92** 460–8
Van de Water S, Safai S, Schippers J M, Weber D C and Lomax A J 2019 Towards flash proton therapy: the impact of treatment planning and machine characteristics on achievable dose rates *Acta Oncol.* **58** 1463–9
Weber D C, Rutz H P, Pedroni E S, Bolsi A, Timmermann B, Verwey J, Lomax A J and Goitein G 2005 Results of spot-scanning proton radiation therapy for chordoma and chondrosarcoma of the skull base: the paul scherrer institut experience *Int. J. Radiat. Oncol.*Biol.*Phys.* **63** 401–9
Wieser H P *et al* 2017 Development of the open-source dose calculation and optimisation toolkit matrad *Med. Phys.* **44** 2556–68
Zenklusen S, Pedroni E and Meer D 2010 A study on repainting strategies for treating moderately moving targets with proton pencil beam scanning at the new gantry 2 at psi *Phys. Med. Biol.* **55** 5103–21
Zhang Y, Huth I, Weber D C and Lomax A J 2018 A statistical comparison of motion mitigation performances and robustness of various pencil beam scanned proton systems for liver tumour treatments *Radiother. Oncol.* **128.1** 182–8
Zhang Y, Huth I, Wegner M, Weber D C and Lomax A J 2016 An evaluation of rescanning technique for liver tumour treatments using a commercial pbs proton therapy system *Radiother. Oncol.* **121** 281–7